Observational evidence for a potential relationship between visible auroral arcs and ion beams - a case study

O. Marghitu[1], A. Blagau[1], J. Vogt[2], B. Klecker[2], G. Haerendel[2], E. Möbius[3], J.P.McFadden[4], C.W.Carlson[4], R. Strangeway[5], and R. Elphic[6]

[1]Institute for Space Sciences, P.O.Box MG-23, Bucharest, R-76900 Romania
[2]Max-Planck-Institut für extraterrestrische Physik, Garching, D-85740 Germany
[3]University of New Hampshire, Durham, NH 03824, US
[4]Space Sciences Lab., Univ. of California, Berkeley, CA 94720, US
[5]Institute for Geophysics and Planetary Physics, UCLA, CA 90024, US
[6]Los Alamos National Lab., NM 87545, US

Observational evidence for a potential relationship between visible auroral arcs and ion beams - a case study

O. Marghitu[1], A. Blagau[1], J. Vogt[2], B. Klecker[2], G. Haerendel[2], E. Möbius[3], J.P.McFadden[4], C.W.Carlson[4], R. Strangeway[5], and R. Elphic[6]

[1]Institute for Space Sciences, P.O.Box MG-23, Bucharest, R-76900 Romania
[2]Max-Planck-Institut für extraterrestrische Physik, Garching, D-85740 Germany
[3]University of New Hampshire, Durham, NH 03824, US
[4]Space Sciences Lab., Univ. of California, Berkeley, CA 94720, US
[5]Institute for Geophysics and Planetary Physics, UCLA, CA 90024, US
[6]Los Alamos National Lab., NM 87545, US

Abstract. Ground optical data in conjunction with particle measurements from FAST orbit 1859 are presented. The satellite crosses the camera field of view for about 2.5 minutes. The recorded data show a large inverted-V with embedded ion beams, pattern most probably resulted from altitude shifts of the lower border of the acceleration region. The optical observations cover a longer period, and enable connection of satellite determined features with later developments of the auroral structure. On this longer time scale small enhancements in the energy flux pumped into ionosphere, coincident with ion beams, seem to amplify and evolve into fully developed visible arcs. Field aligned electron precipitation measured in front of the ion beams together with normal motion of the auroral structure contribute to building up a coherent scenario.

1 Introduction

Optical data have been used for long in studies devoted to both large-scale (e.g. Akasofu, 1968; Anger and Lui, 1973) and small-scale features (e.g. Maggs and Davis, 1968; Meng, 1976) of the aurora.

One distinct topic, given constant attention along the time, refers to the energy source feeding the auroral display. Starting with the pioneering article of McIlwain (1960), the relationship between $\sim 1-10$ keV electrons and the optical signature of aurora was intensively explored (for reviews see Arnoldy, 1974; Meng, 1978). More recently, conjugated studies using ground-based optical and satellite data showed quite convincingly the one-to-one relationship between the auroral arcs and the features of the electron spectra (e.g. Haerendel et al., 1994; Stenbaek-Nielsen et al., 1998).

However, to the knowledge of the authors, there is no study yet trying to establish a relation between ion beams and visible auroral arcs. To avoid confusion we emphasize that we refer to the upward current region. For the downward current

Correspondence to: O. Marghitu, marghitu@fast.nipne.ro

region the relation between ions and aurora has been studied since long time ago (for a review see Hultqvist, 1979).

This is not very surprising. Auroral luminosity is structured into arcs in the upward current region as a direct consequence of energetic electron precipitation. Although the ions take active part in various energization processes (e.g. Shelley et al., 1976; Sharp et al., 1977; Gorney et al., 1981; Reiff et al., 1988; André et al., 1998), the ion effects could be considered as "second order" with respect to light emission. Nevertheless, trying to relate auroral structures and ionospheric ions, in particular ion beams, could offer new insight to auroral processes. It is especially suited to try such an approach at present, when new generations of instruments give better access to small-scale phenomena.

We shall further present a conjunction event between a ground TV camera and the FAST satellite. On the shorter time scale of the satellite pass through the camera's field of view (FoV) the particle measurements suggest the altitude of the acceleration region (AR) changes, in accordance with recent results from FAST (Carlson et al., 1998; McFadden et al., 1999). On the longer time scale of the optical observation one can follow the development of the arc system which reveals a possible relation between ion beams and visible arcs.

2 Instrumentation

2.1 Ground-based cameras

Auroral images were taken with three image-intensified CCD cameras, two of them, Aur-A and Aur-B, equipped with large-angle optics ($86^o \times 64^o$), and one, Aur-D, equipped with narrow-angle optics ($21^o \times 16^o$). During the observations reported here the cameras were operated with > 650 nm edge filters. The images were stored on video tape, at a rate of 25/s if enough luminosity present. The exposure time could be adjusted to either a fraction or a multiple of 40 ms, the standard PAL TV norm. The raw optical data were later digitized to 768×576 pixel arrays with 8-bit depth.
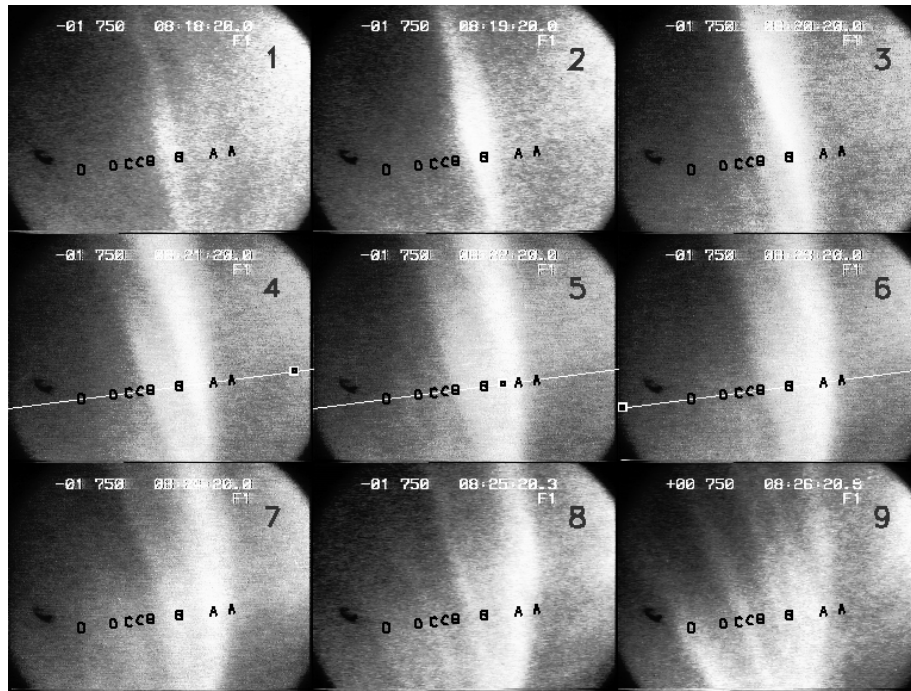
Fig. 1. Selection of auroral images, 1 minute apart, taken with Aur-A on February 9, 1997, UT 8:18–8:26. The North and East directions point roughly to the left and to the bottom, respectively. For better identification the frames are numbered sequentially. FAST crosses the camera's FoV in frames 4,5,6. For these frames the projection of the trajectory is indicated and the satellite's footprint is shown as a square. The limits of the ion beams seen by FAST are overplotted in all the frames (see text).

2.2 Satellite detectors

FAST is equipped with state-of-the art detectors, for both plasma and field observations. The very high resolution permits a detailed study of small-scale phenomena, in particular of ion-beam events. For this paper we use data coming from the electron (EESA) and ion (IESA) spectrometers (Carlson and McFadden, 1998). The energy range of the two instruments is 4 eV – 30 keV and 3 eV – 25 keV respectively, divided into 48 channels. A complete energy sweep is done in 78 ms and a typical temporal resolution during the auroral oval crossing is 312 ms (4 energy sweeps are grouped together). The instruments ensure permanent full pitch-angle coverage, with a resolution of $5.62°$. Data from the tri-axial flux-gate magnetometer (Elphic et al., 1998) were also used, to double-check the upward/downward character of the current.

3 Data description

3.1 Optical data

Ground images in conjunction with FAST were obtained on 9th and 13th of February '97, during an auroral campaign at Deadhorse (Lat. $70.22°$, Lon. $211.61°$), Alaska. In this study we focus on the first event, which took place between UT 8:21:00 and 8:23:20. The optical data used come from Aur-A and cover a longer time interval, UT 8:18 - 9:14. A sequence of 9 frames, 1 minute apart, centered on the conjunction interval, is shown in Fig. 1. The 1 minute resulted by visual evaluation as a reasonable time-scale for the change of the auroral display. The frames are sequentially numbered in the upper right corner, for better readability. One can also

read, in the upper left corner, the exposure time: "00" means 40 ms and "-01" means 20 ms. Note that the exposure time doubles for the last frame.

For the time period when FAST crossed the camera's FoV (frames 4,5,6) we indicated the satellite's footprint at ionospheric level (110 km). The instantaneous satellite's position is shown as a square (the mapping viewing-direction ↔ image-pixel was done by recording reference frames with bright, well-known stars). One can test that the FAST footprint is at the right place: the time for the maximum energy flux, as derived from brightness data, is close to that derived from EESA data (Fig. 2). Cross-correlation of the two data arrays produces a good agreement, within a limit of 2-3 s.

The energy fluxes in Fig. 2 are given in relative units. An absolute calibration of the cameras can also, in principle, be achieved. However, the footprint of FAST path is far from the magnetic zenith ($45°$ maximum elevation while the magnetic zenith is $80°$), so that brightness cannot be directly compared to energy flux. The off zenith trajectory of FAST is also the reason for the discrepancy, except for the maximum, between optical and electron data in Fig. 2.

On each frame in Fig. 1 the ion beams, as read in IESA data (see below), are identified with a letter: A … D. For each ion beam the beginning and the end are indicated. Note that the satellite actually encounters ion beams between 8:22:04 and 8:22:57. Marking of all the frames is only meant to give a better idea about the temporal evolution of luminosity at the places where FAST is going to meet or has met the beams.

For presentation purposes a contrast-enhancement procedure — histogram-equalization — was applied (for details see Research Systems, Inc., 1995). At the same time this procedure partially compensates the loss of brightness when shorter
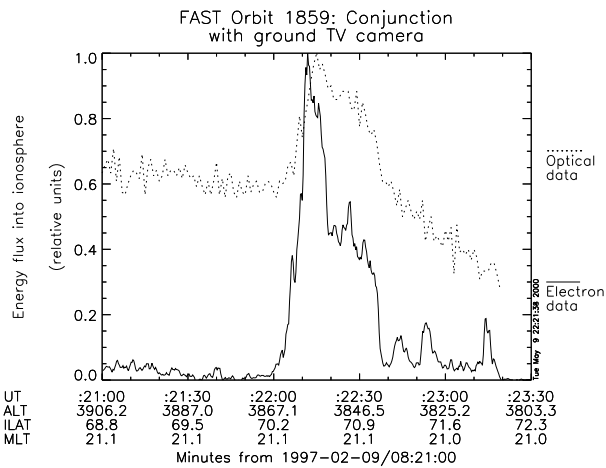
Fig. 2. The energy flux resulting from optical data compared to the energy flux resulting from particle data. The fluxes are represented in relative units, scaled to the maximum value.

exposure times are used and makes the low luminosity structures more evident (on the condition that the exposure time was nevertheless long enough to get something on the tape). The brightness profile, shown in Fig. 2, is not affected by this processing.

3.2 FAST data

During the conjunction FAST was near the apogee, at an altitude of 3800–3900 km. In the upper part of Fig. 3 we present particle and magnetic field data corresponding to the FAST crossing of the camera's FoV. Panels 1 and 3 show energy spectrograms for downgoing electrons and upgoing ions, while panels 2 and 4 show pitch-angle spectrograms for electrons and ions over the whole measured energy range. The most prominent feature in the spectrograms is a large inverted-V which encompasses a multiple ion-beam period. The peak energy is overplotted for both electrons and ions in the respective energy spectrograms, during the ion beam period. Panel 5 shows the perturbation magnetic field three components, oriented roughly N–S, E–W, and along-B. The small N–S and along-B variations correspond to E–W current-sheets, first downward and then upward, which agree well with the particle data.

Electron energy flux and field-aligned (FA) potential are given at the bottom of Fig. 3 for the inverted-V period. The energy flux is mapped at ionospheric level and the full-line curve is corrected to take into account the potential below the satellite during ion beam events:

$$J_E^{corr} = (U_{above} + U_{below})/U_{above} \times J_E$$

U_{above} is taken to be equal to the peak energy of the FA downgoing electrons. U_{below} is calculated the same way from ion spectra. The phenomenological limits of 1 erg/cm^{2}s and 1 keV are overplotted in the respective energy flux and potential panels.
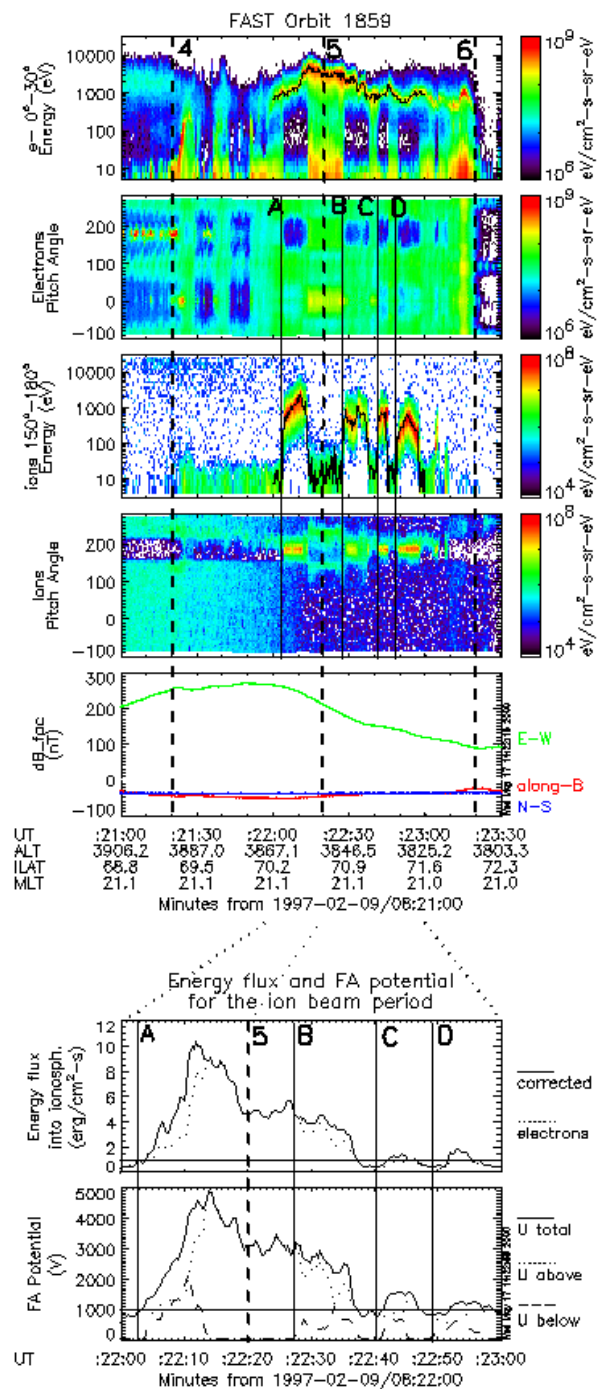

Fig. 3. FAST data, orbit 1859. **Top** Panel 1: Energy spectrogram for downgoing electrons. Panel 2: Electron pitch-angle spectrogram. Panel 3: Energy spectrogram for the upgoing ions. Panel 4: Ion pitch-angle spectrogram. Panel 5: The 3 components of the perturbation magnetic field. The dotted vertical cuts are done at the times of frames "4", "5" and "6" from Fig. 1. The full-line vertical cuts A … D show the times for the plots in Fig. 4. **Bottom** Panel 1: Electron energy flux into ionosphere, mapped at 110 km altitude. The full-line corrects the energy flux during the ion beam events by taking into account the the potential below the satellite. Panel 2: FA potential, bellow the satellite, above the satellite and total. The phenomenological thresholds of 1 erg/cm^{2}s, respectively 1 keV, are also figured.

4 Discussion

On the shorter time scale of the satellite overpass the auroral display is dominated by a large inverted-V arc, roughly 70 km large at ionospheric level (see Fig. 1, frames 4,5,6). The luminosity pattern shows little modification, except for a slow southward motion of the arc. This motion can be noticed by comparing the position of the arc southern edge across the above mentioned frames. The velocity of the motion can be estimated at about 100 m/s. We shall return to this value below.

The satellite data describe the auroral situation in much more detail. For the first part of the overpass one can note in Fig. 3 characteristic features of the downward current region: upward electron beams (panel 2), isotropic, except for the loss-cone, ion precipitation (panel 4), positive slope of the E-W magnetic component (panel 5). All these associate well with the diffuse luminosity area present in Fig. 1 at the southern (right) side. North of this region, between 8:22:00 and 8:23:20, the satellite enters the upward current region, in agreement with the large scale current pattern for the evening sector (Iijima and Potemra, 1978) and crosses a large inverted-V, with embedded ion beams. The repeated encounter of ion beams associated with the optical observation which show a stable situation during the satellite's crossing, suggest that the altitude of the lower border of the AR changes along the satellite path, alternatively passing above and below it, which seems to be a relatively common behavior at the FAST altitude (McFadden et al., 1999, in particular plate 9).

However, on the longer time scale of the image sequence presented in Fig. 1 one can see that the situation is no longer as stable. The auroral display evolved, from one root-arc to a multiple-arc structure. The increased exposure time is partly responsible for the better visibility of the structure multiplicity in the last frame. Nonetheless, as one can see by inspecting the other 8 frames, where the exposure time remained constant, there is a clear evolution independent of instrumental reasons.

As a first step towards establishing a closer connection between the satellite and the optical observation let us look in more detail to the bottom panels of Fig. 3. One can immediately note the close similarity between the energy flux and total implied potential, J_E^{corr} and U_{totsl}, in good agreement with the adiabatic theory of auroral energization (e.g. Knight, 1973; Lyons et al., 1979; Lyons, 1980; Fridman and Lemaire, 1980) and with the large inverted-V character of the auroral structure. An interesting aspect is revealed when relating the data to the phenomenological limits of 1 erg/cm^{2}s and 1 keV. The first one corresponds roughly to the visibility threshold, when looking into the zenith, while the second one is mentioned in various papers as a threshold in auroral electron precipitation (see Semeter et al., 2000, and references therein). It is obvious that both the energy flux and the FA potential come above the respective thresholds at roughly the same time. Incidentally, if one calculates the FA conductivity, $K = J_E/U^2$, resulting from these two values, one gets 10^{-9} S/m^2, a typical value for stable arcs (Olsson et al., 1998, table 1), as it is

also our arc, at least for the duration of the satellite pass.

If we now look more carefully, we can see that, apart from the main arc, there are other two small enhancements of the energy flux, around 22:43 and 22:53 (labeled C and D, in correspondence with the ion beams). They are not visible in the luminosity pattern during the satellite overpass, due to the off zenith position and the short exposure time, set to accommodate the bright main arc. However, about three minutes later (frame 8 in Fig. 1), two new arcs become visible at the respective positions C and D. It is more than plausible that the two energy flux enhancements evolved into fully developed, visible arcs.

More insight to this presumed evolution can be gained by focusing our attention on the ion beams. As an immediate remark, the bottom panels of Fig. 3 suggest a correlation between the ion beam energy and the total potential drop, as well as the association of the ion beams with gradients in the total potential and energy flux. The suggested connection between the evolution of the luminosity pattern and the enhancements in energy flux snapshoted by FAST would thus be extended to ion beams. Such a feature seems to be, however, rather peculiar to the case under study, and is not supported by other FAST data, which apparently shows no correlation between the ion beams and the total potential drop or gradients in this potential drop (McFadden et al., 1998).

Nonetheless, taking into account the optical evidence, it is worth deepening the exploration of the ion beams. A common important feature is the presence of FA electron precipitation just in front of each beam, which is best seen in energy–pitch-angle contour plots. Figure 4 shows a selection of such diagrams, which respectively correspond to the A … D cuts in Fig. 3. It is necessary to mention that **a)** these are not the only measurements showing FA precipitation along the satellite path and **b)** the extension of such periods varies between about 1 s., in front of beam A, up to about 4 s., completely covering the period between beams B and C. Keeping these two facts in mind we shall further analyze the significance of the FA precipitation preceding the ion beams.

Association of FA electrons and upgoing ions has already been observed by the S3-3 spacecraft (Temerin et al., 1981; Mizera et al., 1982; Redsun et al., 1985). The sequential appearance of the electrons and ions was interpreted as happening on opposite sides of electrostatic shocks. Later McFadden et al. (1986) attributed FA electron precipitation at the edge of an arc to cold ionospheric electrons convected above the AR and subsequently energized by the FA potential drop. Such a mechanism would imply an electron distribution with a monoenergetic peak, which would match quite well with the sample data in Fig. 4. One apparent difficulty is that only the first FA burst appears at the edge, all the others come under the large inverted-V. This difficulty can be overcome by taking into account the varying altitude of the lower border of the AR, which makes possible a similar mechanism each time FAST passes from below this lower border to above it. Preliminary analysis show in addition that during ion beam periods the upper border of AR comes quite close to the satellite, so that accelerated electrons have just a short way to travel up
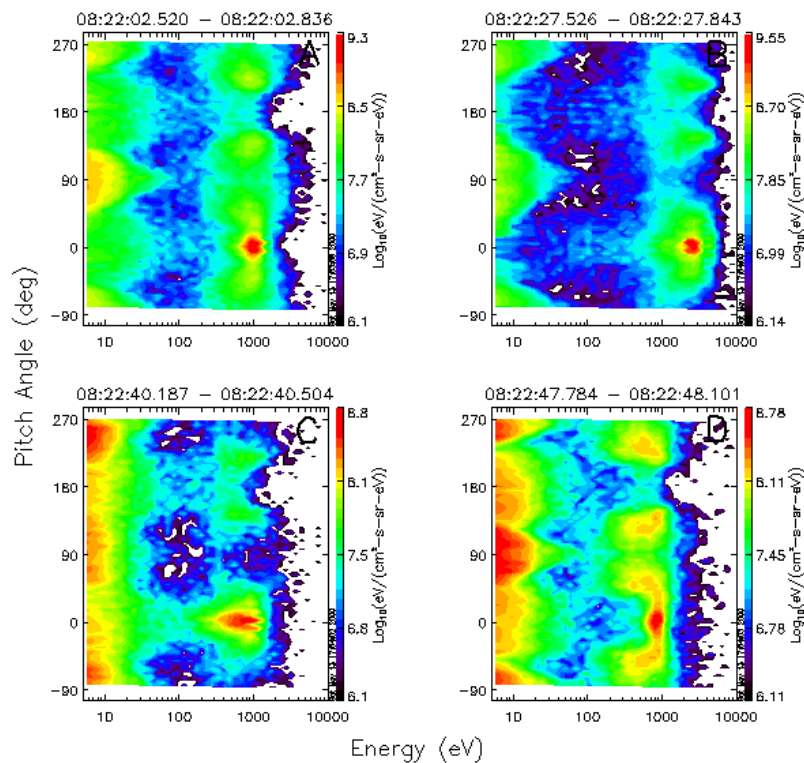
Fig. 4. Energy–pitch-angle distribution snapshots for electrons, shortly before each of the four ion beams.

to detection, which prevent the frequently observed flattening of the distribution.

Further support to a coherent view of the observed optical and particle features comes when considering the estimated 100 m/s normal velocity of the auroral structure. In a series of papers Haerendel (1989, 1994, 1999) suggested a model for the acceleration of the auroral particles which naturally implies the normal motion of the arc. In this model the kinetic energy of the electrons is supplied by conversion of magnetic energy, at the level of the AR. If the input energy is larger or smaller than the output energy, the auroral current circuit expands or shrinks, which produces the motion of the arc. Ionospheric plasma is thus accelerated at the leading edge of the arc, appearing as FA electron precipitation, coming from above, and ion beams, coming from below. The predicted proper motion of the arcs is in close agreement with the experimental measurements (Haerendel et al., 1993; Frey et al., 1996), but one has to be careful when comparing to the model: the normal velocity refers to the motion of the arc in the reference system of the ambient plasma, i.e. in order to get it one has to subtract the plasma velocity - e.g. radar determined - from the velocity of the arc. There is no radar measurement available for the period and location referred to in this study, but except for this the data are in good agreement with the model.

As a final point, the main goal of this study is to show observations suggesting that a more than accidental connection could exist between visible auroral arcs and ion beams.

To put the observation on a sound basis, work is currently done towards a full exploiting of the information contained in the distribution functions provided both by the EESA / IESA spectrometers, as well as by the mass spectrometer aboard FAST (TEAMS, Klumpar et al., 1998). Important results which are expected from the detailed analysis of the distribution functions include a good identification of the various plasma populations and a reasonable evaluation of the altitudinal limits of the AR, implicitly of the electric field distribution along the magnetic field line.

5 Concluding remarks

Optical data from a ground-based camera, in conjunction with FAST data, for one auroral overpass, were investigated. The satellite data were interpreted in terms of the altitude shift of the lower border of the acceleration region. FA electron precipitation in front of the ion beams is consistent both with this altitude variation and with the normal motion of the arc, visible in the optical data. Following the luminosity pattern on the longer time scale of the optical observation suggests a possible relation between ion beams and visible auroral arcs.

References

Akasofu, S.-I., *Polar and Magnetospheric Substorms*, D. Reidel, Dordrecht, Netherlands, 1968.

André, M., Norqvist, P., Andersson, L., Eliasson, L., Eriksson, A., Blomberg, L., Erlandson, R., and Waldemark, J., Ion energization mechanisms at 1700 km in the auroral region, *J. Geophys. Res.*, *103*, 4199–4222, 1998.

Anger, C. and Lui, A., A global view at the polar region on December 18, 1971, *Planet. Space Sci.*, *21*, 783, 1973.

Arnoldy, R., Auroral particle precipitation and Birkeland currents, *Rev. Geophys. Space Phys.*, *12*, 217, 1974.

Carlson, C. and McFadden, J., Design and application of imaging plasma instruments, in *Measurement Techniques in Space Plasmas*, p. 125, AGU, 1998.

Carlson, C., Pfaff, R., and Watzin, J., The Fast Auroral SnapshoT mission, *Geophys. Res. Lett.*, *25*, 2013–2016, 1998.

Elphic, R., Means, J., Snare, R., Strangeway, R., Kepko, L., and Ergun, R., Magnetic field instruments for the Fast Auroral Snapshot Explorer, *Submitted to Space Sci. Rev.*, 1998.

Frey, H., Haerendel, G., Knudsen, D., Buchert, S., and Bauer, O., Optical and radar observations of the motion of auroral arcs, *J. Atmos. Terr. Phys.*, *58*, 57, 1996.

Fridman, M. and Lemaire, J., Relationship between auroral electrons fluxes and field aligned potential differences, *J. Geophys. Res.*, *85(A2)*, 664–670, 1980.

Gorney, D., Clarke, A., Croley, D., Fennell, J., Luhmann, J., and Mizera, P., The distribution of ion beams and conics below 8000 km, *J. Geophys. Res.*, *86*, 83–89, 1981.

Haerendel, G., Cosmic linear accelerators, in *Proc. Varenna-Abastumani Int. School & Workshop on Plasma Astrophysics*, p. 37, ESA SP-285, Varenna, Italy, 1989.

Haerendel, G., Acceleration from field-aligned potential drops, *Astrophys. J. Suppl. Ser.*, *90*, 765, 1994.

Haerendel, G., Origin and dynamics of thin auroral arcs, *Adv. Space Res.*, *23*, 1637–1645, 1999.

Haerendel, G., Buchert, S., La Hoz, C., Raaf, B., and Rieger, E., On the proper motion of auroral arcs, *J. Geophys. Res.*, *98*, 6087, 1993.

Haerendel, G., Frey, H., Bauer, O., Rieger, E., Clemmons, J., Boehm, M., Wallis, D., and Lühr, H., Inverted-V events simultaneously observed with Freja satellite and from the ground, *Geophys. Res. Lett.*, *21*, 1891, 1994.

Hultqvist, B., The hot ion component of the magnetospheric plasma and some relations to the electron component – observations and physical implications, *Space Sci. Rev.*, *23*, 581, 1979.

Iijima, T. and Potemra, T., Large-scale characteristics of field-aligned currents associated with substorms, *J. Geophys. Res.*, *83*, 599–615, 1978.

Klumpar, D., Möbius, E., Kistler, L., Popecki, M., Crocker, K., Granoff, M., Tang, L., Carlson, C., McFadden, J., Klecker, B., Eberl, F., Künneth, E., Kästle, H., Peterson, W., Shelley, E., and Hovestadt, D., The Time-of-flight Energy, Angle, Mass Spectrograph (TEAMS) experiment for FAST, *Submitted to Space Sci. Rev.*, 1998.

Knight, S., Parallel electric fields, *Planet. Space Sci.*, *21*, 741, 1973.

Lyons, L., Generation of large-scale regions of auroral currents, electric potentials, and precipitation by the divergence of the convection electric field, *J. Geophys. Res.*, *85*, 17–24, 1980.

Lyons, L., Evans, D., and Lundin, R., An observed relation between magnetic field aligned electric fields and downward energy fluxes in the vicinity of auroral forms, *J. Geophys. Res.*, *84(A2)*, 457, 1979.

Maggs, J. and Davis, T., Measurements of the thickness of auroral structures, *Planet. Space Sci.*, *16*, 205, 1968.

McFadden, J., Carlson, C., and Boehm, M., Field-aligned electron precipitation at the edge of an arc, *J. Geophys. Res.*, *91*, 1723–1730, 1986.

McFadden, J., Carlson, C., R.E.Ergun, Mozer, F., Temerin, M., Peria, W., Klumpar, D., Shelley, E., Peterson, W., Möbius, E., Kistler, L., Elphic, R., Strangeway, R., Cattell, C., and Pfaff, R., Spatial structure and gradients of ion beams observed by FAST, *Geophys. Res. Lett.*, *25*, 2021–2024, 1998.

McFadden, J., Carlson, C., and R.E.Ergun, Microstructure of the auroral acceleration region as observed by FAST, *J. Geophys. Res.*, *104*, 14 453–14 480, 1999.

McIlwain, C., Direct measurement of particles producing visible auroras, *J. Geophys. Res.*, *65*, 2727–2747, 1960.

Meng, C., Simultaneous observations of low-energy electron precipitation and optical auroral arcs in the evening sector by the DMSP-32 satellite, *J. Geophys. Res.*, *81*, 2771, 1976.

Meng, C.-I., Electron precipitation and polar aurora, *Space Sci. Rev.*, *22*, 223, 1978.

Mizera, P., Gorney, D., and Fennell, J., Experimental verification of an S-shaped potential structure, *J. Geophys. Res.*, *87*, 1535–1539, 1982.

Olsson, A., Andersson, L., Eriksson, A., Clemmons, J., Erlandsson, R., Reeves, G., Hughes, T., and Murphree, J., Freja studies of the current–voltage relation in substorm related events, *J. Geophys. Res.*, *103*, 4285–4301, 1998.

Redsun, M., Temerin, M., and Mozer, F., Classification of auroral electrostatic shocks by their ion and electron associations, *J. Geophys. Res.*, *90*, 9615–9633, 1985.

Reiff, P., Collin, H., Craven, J., Burch, J., Winningham, J., Shelley, E., Frank, L., and Friedman, M., Determination of auroral electrostatic potentials using high- and low-altitude particle distributions, *J. Geophys. Res.*, *93*, 7441–7465, 1988.

Research Systems, Inc., *IDL Reference Guide*, p. 470, Boulder, Colorado, 1995.

Semeter, J., Vogt, J., Harendel, G., Lynch, K., and Arnoldy, R., Persistent suprathermal electron precipitation: evidence for ionospheric regulation of discrete aurora, *Submitted to J. Geophys. Res.*, 2000.

Sharp, R., Johnson, R., and Shelley, E., Observation of an ionospheric acceleration mechanism producing energetic (kev) ions primarily normal to the geomagnetic field direction, *J. Geophys. Res.*, *82*, 3324–3328, 1977.

Shelley, E., Sharp, R., and Johnson, R., Satellite observations of an ionospheric acceleration mechanism, *Geophys. Res. Lett.*, *3*, 654–657, 1976.

Stenbaek-Nielsen, H., Hallinan, T., Osborne, D., Kimball, J., Chaston, C., McFadden, J., Delory, G., Temerin, M., and Carlson, C., Aircraft observations conjugate to FAST: Auroral arc thicknesses, *Geophys. Res. Lett.*, *25*, 2073, 1998.

Temerin, M., Cattell, C., Lysak, R., Hudson, M., Torbert, R., Mozer, F., Sharp, R., and Kintner, P., The small-scale strucuture of electrostatic shocks, *J. Geophys. Res.*, *86*, 11 278–11 298, 1981.